

See discussions, stats, and author profiles for this publication at: <https://www.researchgate.net/publication/281067531>

Pseudohalide (SCN⁻)-doped MAPbI₃ perovskites: A few surprises

ARTICLE *in* JOURNAL OF PHYSICAL CHEMISTRY LETTERS · AUGUST 2015

Impact Factor: 7.46 · DOI: 10.1021/acs.jpclett.5b01327

CITATION

1

READS

68

7 AUTHORS, INCLUDING:



Ansuman Halder

Indian Institute of Technology Bombay

6 PUBLICATIONS 53 CITATIONS

[SEE PROFILE](#)



Anand Selvin Subbiah

Indian Institute of Technology Bombay

14 PUBLICATIONS 65 CITATIONS

[SEE PROFILE](#)



Shyamtanu Chattoraj

Indian Association for the Cultivation of Scie...

18 PUBLICATIONS 93 CITATIONS

[SEE PROFILE](#)



Arindam Chowdhury

Indian Institute of Technology Bombay

38 PUBLICATIONS 707 CITATIONS

[SEE PROFILE](#)

Pseudohalide (SCN^-)-Doped $MAPbI_3$ Perovskites: A Few Surprises

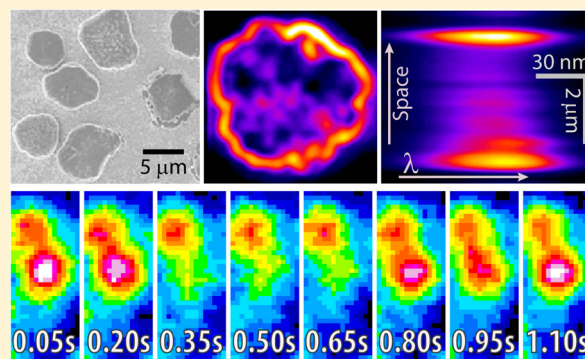
Ansuman Halder,[‡] Ramya Chulliyil,[†] Anand S Subbiah,[‡] Tuhin Khan,[†] Shyamtanu Chattoraj,[§] Arindam Chowdhury,^{*,†} and Shaibal K Sarkar^{*,‡}

[‡]Department of Energy Science and Engineering and [†]Department of Chemistry, Indian Institute of Technology Bombay, Powai, Mumbai 400076, India

[§]Department of Physical Chemistry, Indian Association for the Cultivation of Science, Jadavpur, Kolkata 700032, India

Supporting Information

ABSTRACT: Pseudohalide thiocyanate anion (SCN^-) has been used as a dopant in a methylammonium lead tri-iodide ($MAPbI_3$) framework, aiming for its use as an absorber layer for photovoltaic applications. The substitution of SCN^- pseudohalide anion, as verified using Fourier transform infrared (FT-IR) spectroscopy, results in a comprehensive effect on the optical properties of the original material. Photoluminescence measurements at room temperature reveal a significant enhancement in the emission quantum yield of $MAPbI_{3-x}(SCN)_x$ as compared to $MAPbI_3$, suggestive of suppression of nonradiative channels. This increased intensity is attributed to a highly edge specific emission from $MAPbI_{3-x}(SCN)_x$ microcrystals as revealed by photoluminescence microscopy. Fluorescence lifetime imaging measurements further established contrasting carrier recombination dynamics for grain boundaries and the bulk of the doped material. Spatially resolved emission spectroscopy on individual microcrystals of $MAPbI_{3-x}(SCN)_x$ reveals that the optical bandgap and density of states at various (local) nanodomains are also nonuniform. Surprisingly, several (local) emissive regions within $MAPbI_{3-x}(SCN)_x$ microcrystals are found to be optically unstable under photoirradiation, and display unambiguous temporal intermittency in emission (blinking), which is extremely unusual and intriguing. We find diverse blinking behaviors for the undoped $MAPbI_3$ crystals as well, which leads us to speculate that blinking may be a common phenomenon for most hybrid perovskite materials.



Over the last six decades, the field of photovoltaics has witnessed numerous kinds of materials with diversified architectures that endorse promise toward cleaner energy. During the last couple of years, a newer class of absorber material in the form of hybrid organic–inorganic perovskite structure has shown unprecedented progress in light-to-energy conversion efficiencies, either used as flat heterostructure or under bulk-heterojunction configuration.^{1–3} In general, the term perovskites represents a wide class of materials that are generally inorganic and in the form of ABX_3 , where A and B are usually metals, and X is oxygen or halogens. However, the material responsible for the recent sensation in photovoltaics belongs to an overlapping subset of metal organic frameworks with Perovskite structure, for example, methylammonium lead iodide ($MAPbI_3$). This material and its analogues exhibit an array of properties such as ambi-polar charge transport, high absorption coefficient and reasonably good electron/hole diffusion length, making them appropriate for photovoltaic applications.^{4–8} The ease of synthesis and low temperature crystallization suits well for its applicability in low cost photovoltaic devices with high efficiencies. Apart from the inherent toxicity due to the use of lead (Pb) in the material, these materials are also a bit underprivileged in terms of stability as of now.^{9,10}

The use of formamidinium cation replacing methyl amine group has been reported to improve the stability of the material to certain extent.¹¹ Very recently, Jiang et al., showed improved stability by incorporating pseudohalide that replaces the halide ions in the tetragonal sites of the perovskite unit lattice.¹² The pseudohalide thiocyanate (SCN^-) anion has an effective ionic radii of ~217 pm, which is relatively closer to that of iodine's effective ionic radii of 220 pm and is expected to substitute a fraction of iodine atoms in the parent material ($MAPbI_3$).¹³ In this letter, we introduce a pseudohalide molecular anion, SCN^- , as a dopant in $MAPbI_3$ structure as opposed to that reported by Jiang et al.¹² Lead thiocyanate $Pb(SCN)_2$ is used as the precursor material to synthesize this chromophore and the change in optical and electronic properties of the parent material ($MAPbI_3$) upon introduction of SCN^- ($MAPbI_{3-x}(SCN)_x$) anion is studied. This material is tested for its photovoltaics performance using mesoscopic titania as scaffold/electron-transport layer and Spiro-OMeTAD as hole transport layer under standard illumination conditions. We show that

Received: June 22, 2015

Accepted: August 17, 2015

incorporation of *pseudo*-halide anion as dopants in the MAPbI₃ structure severely affects optoelectronic properties of the host material. As compared to MAPbI₃, the optical band gap of the SCN⁻ doped material MAPbI_{3-x}(SCN)_x is increased by ~80 meV, accompanied by a remarkable enhancement in the photoluminescence (PL) emission quantum yield.

Interestingly, a recent report by deQuilettes et al.¹⁴ has shown the existence of a significant spatial variation in PL intensity and carrier lifetime, particularly at the grain boundaries in comparison to the bulk of the material in individual grains of crystalline films made of nonstoichiometric organic-inorganic [CH₃NH₃PbI_{3-x}(Cl)_x] perovskites. Such differences in PL intensity have been attributed to the contiguous variation in radiative and nonradiative recombination dynamics. In contrast, using spectrally resolved PL microscopy, here we show that the emission intensity (or radiative recombination efficiency) is substantially *higher* at the grain boundaries of MAPbI_{3-x}(SCN)_x as compared to the interior regions of the crystals. PL lifetime imaging microscopy demonstrates considerable diversity in carrier recombination dynamics between the edges and the bulk of the crystal. Moreover, our measurements reveal spatially heterogeneous spectral properties of various nanodomains within individual MAPbI_{3-x}(SCN)_x crystals. Finally, we show that local emissive domains within perovskite microcrystals undergo unambiguous dynamical fluctuations in emission between multiple intensity levels, reminiscent of PL intermittency (or *blinking*) known to occur for single emitters.¹⁵

Lead thiocyanate and methylammonium iodide (MAI) are dissolved in *N,N'*-dimethylformamide (DMF) in a series of molar ratios ranging from 1:1 to 1:5. The solution is spin coated on porous Al₂O₃ coated (~500 nm thick) glass substrate or coverslips to form a thin film, depending upon the need of the specific measurement. Films are then subsequently annealed 363 K resulting in the formation of MAPbI_{3-x}(SCN)_x perovskites. It is observed that a Pb(SCN)₂ to MAI ratio of 1:1 and 1:2 results in complete conversion to the perovskite structure, while a poorly crystalline perovskite material is formed when a ratio of 1:3 (Pb(SCN)₂:MAI) is maintained. When the precursors are subjected to a 1:4 molar ratio, it resulted in a highly crystalline material with an extinction coefficient similar to that of MAPbI₃. Further increase in the MAI molar concentration results in poor quality material formation. More details on the material fabrication methodology and the effect of various molar ratios in the film formation (Figure S1) are provided in the *Supporting Information* (SI). From the *in situ* X-ray diffraction (XRD) study, it is observed that the material MAPbI_{3-x}(SCN)_x (1:4) can be obtained at and beyond an annealing temperature of 333 K. However, to maintain the consistency in comparison with MAPbI₃, we have kept annealing temperatures of both samples at 363 K. All details on materials, measurements, and characterization techniques are provided in the SI.

The X-ray diffraction patterns of MAPbI_{3-x}(SCN)_x and the host MAPbI₃ material is shown in Figure 1. The MAPbI₃ peaks obtained here exactly match with the existing literature.¹⁶ It is evident from Figure 1 that all major signature peaks of MAPbI_{3-x}(SCN)_x are slightly shifted toward a lower 2θ value (see inset; ~0.2° shift for 110 peak) in comparison to the host material. Similar shift in the XRD peak position has been also found when chlorine was incorporated in the host MAPbI₃, forming MAPbI_{3-x}Cl_x.¹⁷ This elucidates the presence of a uniform strain throughout the lattice of the material due to

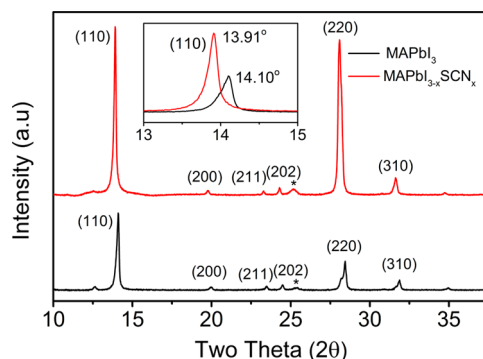


Figure 1. XRD patterns of MAPbI₃ and MAPbI_{3-x}(SCN)_x obtained at room temperature.

SCN incorporation. We also clearly observe the presence of a strong SCN stretch¹⁸ at 2060 cm⁻¹ in the Fourier transform infrared (FT-IR) spectra that is completely absent in the parent perovskite material¹⁹ (Figure S2, SI). These observations strongly suggest that SCN anions have been incorporated in the bulk of MAPbI₃ material resulting in the formation of MAPbI_{3-x}(SCN)_x.

To understand the changes in electronic structure of the pseudohalide anion-doped variant with respect to the host material, optical absorption and PL emission spectroscopy were performed on MAPbI₃ and MAPbI_{3-x}(SCN)_x under both ambient and cryogenic conditions (Figure 2). At 298 K (Figure 2a), the absorption band edge onset of the undoped host material is located at ~790 nm, and we estimate (using a tauc plot) the corresponding band gap to be 1.57 eV, in accordance with prior reports.^{20,21} Upon doping MAPbI₃ with SCN, the absorption band edge onset undergoes a blue shift of ~40 nm, and the corresponding band gap is estimated to be ~1.65 eV. We note that the slope of the absorption edge from its onset varies widely between both materials, i.e., the doped perovskite has relatively shallow absorption edge (i.e., broader spectral width) as compared to the host, indicating the presence of defect or tail states. In addition, the optical absorption spectra suggest that the incorporation of SCN results in considerable reduction of the molar extinction coefficient, which was further confirmed by absorptance measurements. The room-temperature PL emission spectra for both the materials (Figure 2a, solid lines) were acquired by excitation at 480 nm using a halogen light source coupled with monochromator. Interestingly, in spite of the much lower extinction coefficient for the doped material, MAPbI_{3-x}(SCN)_x exhibits more than 10-fold enhanced PL emission as compared to that of the host MAPbI₃, which suggests a much higher radiative recombination efficiency in the thiocyanate-doped perovskite. The room temperature PL peak position of MAPbI₃ is centered at 776 nm (1.597 eV), while that for MAPbI_{3-x}(SCN)_x is slightly blue-shifted, with the peak located at 756 nm (1.64 eV), consistent with earlier reports.^{20,22} We also find that at 295 K, MAPbI_{3-x}(SCN)_x exhibits much larger (~125 meV) Stokes shift as compared to that for MAPbI₃ (~22 meV), which can arise from a variety of reasons such as excitation migration to low energy levels, dopant induced configurational energetic disorder in the host or relaxation in the lattice which can cause polaronic effects.^{22,23}

We noticed that the PL emission spectral profiles (Figure 2a) for both the host and the doped perovskite materials are unsymmetrical and skewed to the higher energy side, which

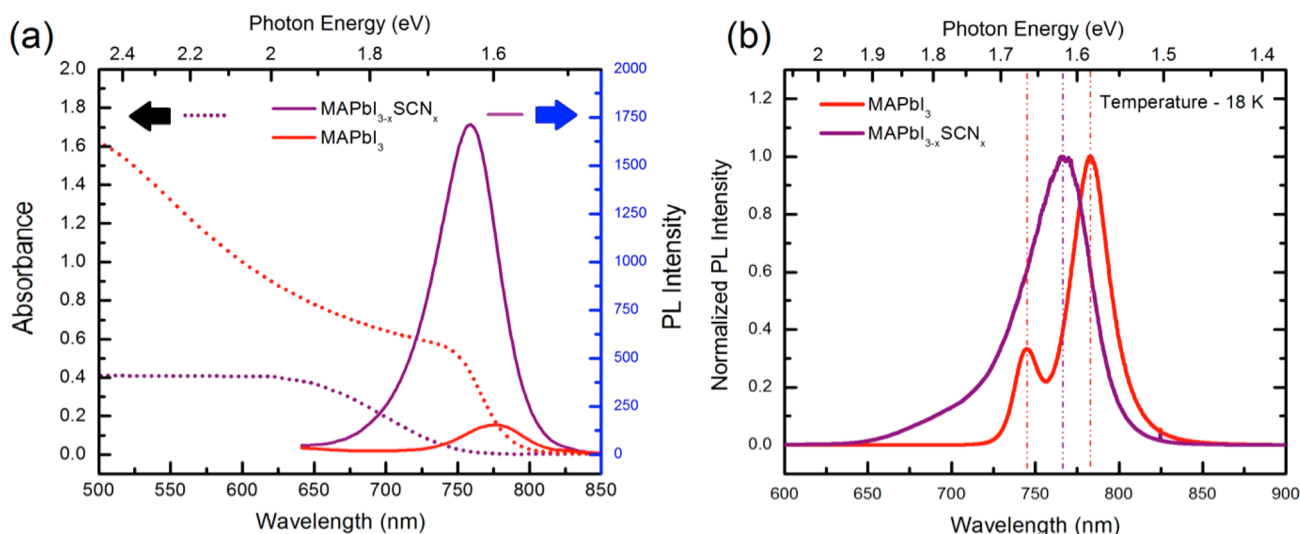


Figure 2. (a) UV–vis absorption and PL emission spectrum of MAPbI₃ and MAPbI_{3-x}(SCN)_x at room temperature (295 K). (b) Normalized PL emission of MAPbI₃ and MAPbI_{3-x}(SCN)_x at 18 K.

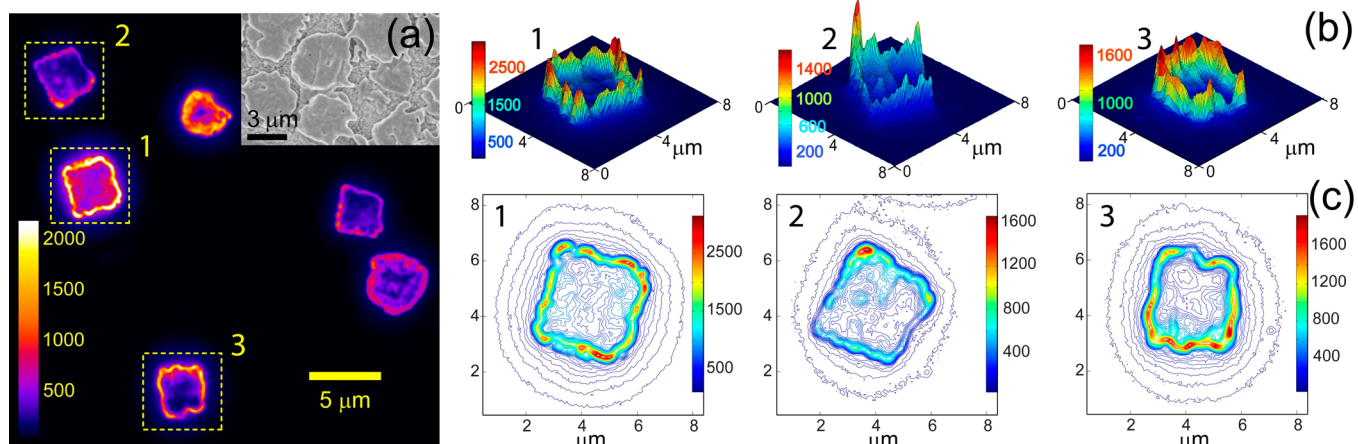


Figure 3. (a) PL intensity image of spatially separated MAPbI_{3-x}(SCN)_x micro crystals spin-cast on a glass substrate. Inset shows a SEM image of the same sample at a higher concentration. (b) 3D rendition of intensity profiles for three individual micro crystals marked 1–3 (dotted squares) in panel a. (c) Intensity contour plots depicting the remarkable spatial variation in radiative recombination efficiency within individual microcrystals (1–3). Intensity calibration bars (color coded) in all images are in counts per second (cps).

suggests the existence of multiple transitions buried underneath the broad emission envelopes. To detect such underlying transitions, PL emission spectroscopy was performed under cryogenic conditions using a laser excitation at 532 nm (Figure 2b). For the host MAPbI₃ material, two transitions at \sim 744 nm (1.67 eV) and \sim 783 nm (1.58 eV) can be resolved at 18 K, which could be fit to two Gaussians (Figure S3, SI). The lower energy transition (\sim 1.58 eV) is located at a very similar energetic position as that at room temperature (\sim 1.59 eV), which suggests that this peak originates from the same interband transition. The much narrower spectral line width (\sim 50 meV) for the host material as compared to 295 K is expected from reduction of phonon population at low temperatures.^{24,25}

Interestingly, the cryogenic emission spectral envelope for the MAPbI_{3-x}(SCN)_x perovskite material is nominally different from that at room temperature, with comparable line width (\sim 100 meV) and a slight blue-shift of \sim 20 meV. While the two transitions could not be resolved even at 18 K, the shoulder at the blue edge of the transition band is clearly more prominent

as compared to that at 295 K. The inability to resolve the two transitions even at 18 K also raises the question on spatially heterogeneous (site specific) emission from the doped perovskite material. To elucidate such a possibility in MAPbI_{3-x}(SCN)_x, PL microscopy measurements were performed under conditions such that crystalline islands (grains) of the material is spatially segregated when spin-cast out of solution on a silica substrate. Figure 3 shows a characteristic PL intensity image of MAPbI_{3-x}(SCN)_x crystals under 532 nm laser excitation, obtained using a home-built spectrally resolved epi-fluorescence microscopy setup^{26,27} (for details, see SI). The morphology of the crystalline grains observed in the PL images are similar to that obtained from scanning electron microscopy (SEM; Figure 3a (inset) and Figure S4, SI), with irregular shaped disks of dimensions ranging between 3 and 6 μ m. Clearly, the MAPbI_{3-x}(SCN)_x crystals are typically found to be much more emissive (>10 times) as compared to MAPbI₃ crystals (Figure S5, SI), consistent with ensemble PL measurements (Figure 2a). More importantly, PL imaging reveals that there is a dramatic difference of spatial distribution

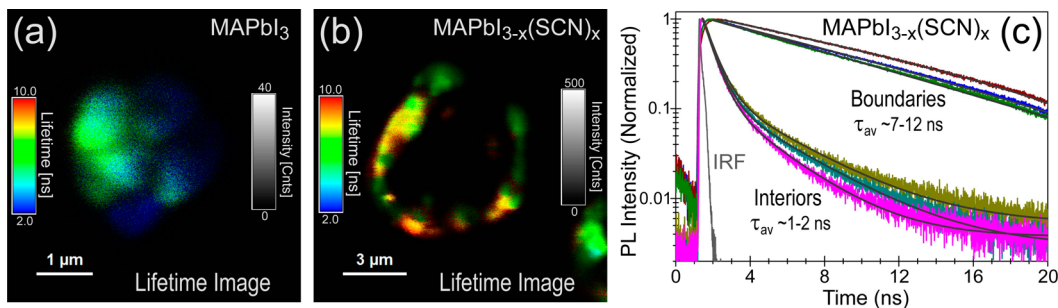


Figure 4. Intensity-weighted PL lifetime images of spatially isolated microcrystalline grains of (a) MAPbI₃ and (b) MAPbI_{3-x}(SCN)_x, collected using a pulsed laser excitation at 470 nm and a bandpass filter (730–780 nm), up to a time-delay of 20 ns (c) Representative PL decay from three regions at the interiors and boundaries of SCN-doped perovskite crystals. Black lines are single exponential (boundaries) and biexponential (interiors) fits to time-resolved PL decay.

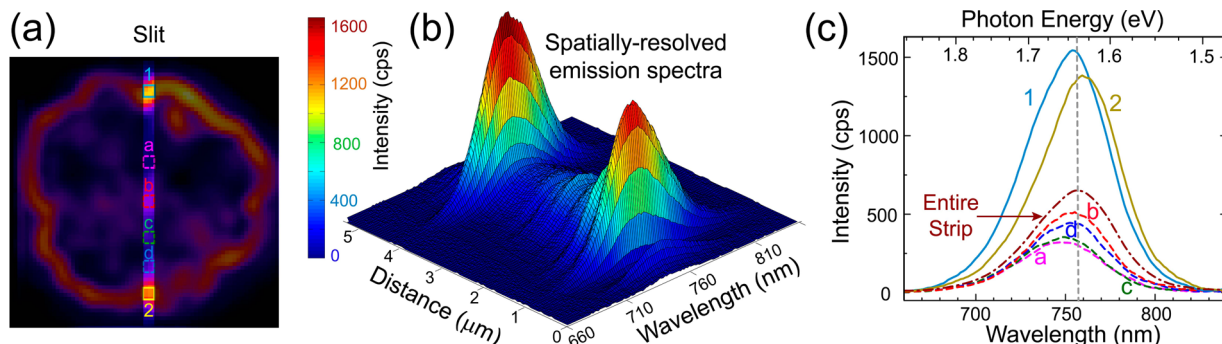


Figure 5. Spatially resolved PL emission spectroscopy from nanodomains within a single MAPbI_{3-x}(SCN)_x crystal. (a) PL image of a crystal through a narrow slit via which emission spectra was collected. (b) Intensity color coded 3D profile of the spectrally resolved image obtained through slits as shown in panel a. (c) Spatially resolved emission spectra from nanodomains at boundaries (solid lines, marked 1–2 in panel a) and interior (dashed lines, marked a–d in panel a) of the microcrystal, along with spatially averaged PL spectra (dashed-dotted line) for the entire vertical strip.

of emission behaviors within individual crystals; as opposed to the MAPbI₃ (Figure S5a, SI), for the vast majority of MAPbI_{3-x}(SCN)_x microcrystals (Figure 3a, and Figure S5b, SI), the emission originating from the edges (or grain boundaries) are typically much more intense as compared to that from interior regions (bulk) of the crystals. The spatial nonuniformity of emission characteristics are shown in 3D intensity profiles (Figure 3b) and contour plots (Figure 4c) for three individual crystals (marked 1–3 in Figure 3a), from which it is evident that even different local nanodomains at the boundaries have highly inhomogeneous emission. We note that the PL images (Figure 3) are consistent with SEM images (Figure 3a (inset), and Figure S4, SI) which depict higher contrast at the grain boundaries of the doped crystals, and suggests significant differences in optoelectronic properties at the interior and edge regions of the pseudohalide-doped MAPbI₃.

To explore (spatial) variability of carrier recombination (CR) dynamics within interior regions and boundaries as well as the effect of SCN doping, fluorescence lifetime imaging microscopy (FLIM) was performed on individual microcrystals of MAPbI₃ and MAPbI_{3-x}(SCN)_x under ambient conditions. Analysis of FLIM images (Figure 4a,b) reveal that the average radiative lifetime (τ_{av}) of individual MAPbI₃ crystals are typically between 1 and 4 ns. It should be mentioned that even for the undoped MAPbI₃ crystals, we observed both single and biexponential (SI Figure S6) decay of photoexcited carriers (from different spatial zones), although there is no particular spatial dependence of the nature of CR dynamics. This suggests that CR can occur via at least two mechanisms for different

locations of the MAPbI₃ crystal, i.e., either through bimolecular (electron–hole) recombination or via trap-assisted radiative recombination processes.^{28,29} In contrast, the SCN-doped perovskite exhibit considerably diverse CR dynamics with a clear spatial correspondence for various zones within each crystal (Figure 4b,c). At the boundaries where emission intensities are high, the vast majority of the locally emissive regions exhibit a slow, near-single exponential PL decay with lifetimes ranging between 7 and 12 ns, while at the interior (dark) regions, CR processes typically follow biexponential behaviors with a dominant sub-nanosecond fast component and a lesser contributing slow component (~2–5 ns), which results in a τ_{av} typically between 1 and 2 ns. Such biexponential PL decay with dominant fast component indicates the high density of nonradiative traps (chemical or structural defects) within the interior regions for the doped MAPbI₃. Further, much slower single-component decay at the boundaries suggests the presence of long-lived trap states that assist in radiative recombination of charge carriers, which likely causes enhanced emission from the edges.

It should be noted that the ensemble time-resolved measurements in fact show an opposite trend in terms of CR dynamics, where the PL decays faster in the doped material as compared to MAPbI₃ (Figure S7, Table T1, SI). This is likely due to the prevalence of the bulk material (i.e., interior regions) in micrometer-sized perovskite crystals as compared to the boundary regions. The observed inconsistency of the ensemble and spatially resolved studies also implies that ensemble PL decay on such perovskite materials with spatially inhomogeneous (site specific) emission behaviors might not reflect the

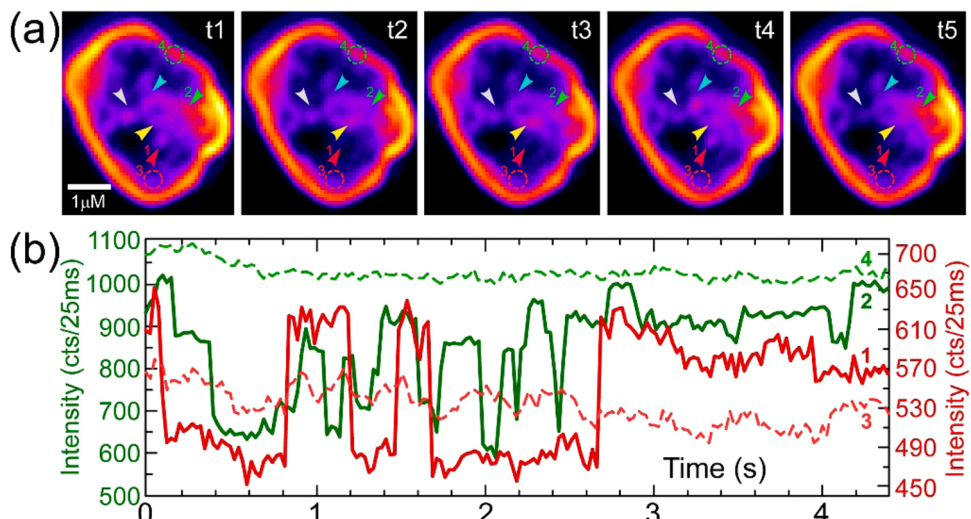


Figure 6. Spatiotemporal dependence of PL intensity within a single $\text{MAPbI}_{3-x}(\text{SCN})_x$ crystal. The PL images (t1 to t5) are selected from 3rd, 30th, 85th, 101st, and 174th frames of the movie M1 provided in the SI showing PL intermittency (blinking) in nanodomains (marked using arrows and circles) within the microcrystal. (b) PL intensity trajectories collected at 35 Hz from nanodomains marked 1–4 in panel a, demonstrating spatial variability in blinking behaviors. The noise from the background signal in the absence of microcrystals show fluctuations of less than 10 cts/25 ms (Figure S8 in the SI).

actual nature of CR mechanisms, and it is imperative to analyze a large number of spatially resolved lifetime data to understand the extent of nonuniformity in CR dynamics. Nonetheless, both lifetime and intensity imaging on individual $\text{MAPbI}_{3-x}(\text{SCN})_x$ microcrystals unambiguously point out to the remarkable diversity in radiative recombination efficiency as well as CR dynamics between the interior of crystalline grains and the boundary regions.

This prompted us to investigate the spatial differences in optical band gap (transition energies) within individual $\text{MAPbI}_{3-x}(\text{SCN})_x$ crystals using spectrally resolved PL microscopy under ambient conditions (Figure 5). A narrow slit was used to spatially resolve the emission along a vertical strip of an isolated crystal as depicted in Figure 5a, following which the dispersed emission spectra of the entire strip (Figure 5b) was collected simultaneously using a transmission grating based spectrograph coupled to a CCD detector.^{26,27} The difference in emission behaviors, both at the boundaries as well as the interior of the microcrystal were exemplified by representative spectral profiles in Figure 5c, and are compared with the spatially averaged emission spectra (dashed-dot line). Interestingly, we find that the entire emission envelopes obtained from two locations at the boundary (marked 1 and 2) are energetically shifted with respect to each other (Figure 5c), and there are similar spatial variations in the transition energies (optical band gap) from interior regions (marked a–d) as well. While we do find that on an average, the emission from the edges (~ 1.625 eV) are slightly lower in energy as compared to that of the interior (~ 1.647 eV), the range as well as standard deviation of transition energies is quite significant as compared to the mean values (Table T1, SI), suggesting considerable spatial heterogeneity in the optical band gap of the doped material. In addition, on an average, the PL emission line widths (which reflect the density of states) obtained from the boundary regions are more narrowly distributed (Table T2, SI) and have slightly lower values (mean of ~ 116 meV) as compared to those from the interior of the crystals (mean of ~ 134 meV). However, for the $\text{MAPbI}_{3-x}(\text{SCN})_x$ crystals that we have investigated, no unequivocal correlation is observed

between optical band gap or density of states with the spatial location of the nanodomains (i.e., interiors and boundaries).

It can be speculated that perhaps, the spatial inhomogeneity in the electronic structure of SCN-doped perovskite crystals results in diverse CR dynamics observed in FLIM measurements. Indeed, the spatial variation in luminescence properties can arise due to compositional variations and, possibly, the extent of doping in various spatial locations. Segregation of dopants to the edges of the crystal may cause such an effect that can potentially alter defect density fluctuation between the edges and the bulk regions of the sample. Another possibility is that the strain in the lattice relaxes mostly at the edges of the crystal, which is perhaps more realistic than only compositional heterogeneity being the cause, and can explain the peak shift in the XRD measurements as well.

Interestingly, apart from large spatial variation of the PL emission in individual $\text{MAPbI}_{3-x}(\text{SCN})_x$ crystals, we find that the emission originating from spatially separated nanodomains is temporally nonuniform, i.e., the local emissive sites within the crystals are optically unstable and undergo irregular oscillatory behaviors, reminiscent of fluorescence intermittency (blinking) in single-emitters. Figure 6a shows temporal snapshots of a single $\text{MAPbI}_{3-x}(\text{SCN})_x$ crystal during a course of continuous illumination. Representative emission intensity traces obtained from four nanodomains within the crystal (marked 1–4) are shown in Figure 6b, from which it is clear that certain regions (marked 1 and 2) exhibit rather prominent temporal fluctuations in PL intensity. We also note that much smaller amplitude intensity fluctuations, higher than the background noise due to CCD (in absence of the crystals, Figure S8, SI) are present throughout the crystal (marked 3 and 4). We find similar blinking behaviors in a majority of $\text{MAPbI}_{3-x}(\text{SCN})_x$ crystals.

While photoinduced blinking behaviors are commonly observed for single semiconductor nanocrystals and fluorescent molecules,^{30,31} and has also been reported for individual radiative recombination centers in quantum-well heterostructures,^{26,32,33} until recently, PL intermittency has been rarely observed in perovskite microcrystals.³⁴ While there are a couple

of reports on relatively large ($\sim\mu\text{m}$) emissive domains within InGaN quantum-well heterostructures undergoing optical instability,^{32,33} these observations are uncommon, and it is quite surprising that such a high density of local submicroscopic domains within these perovskite crystals of several micrometers exhibits such unambiguous PL intermittency. More importantly, the nature of optical instability observed for $\text{MAPbI}_{3-x}(\text{SCN})_x$ crystals is also quite different from single emitters, where fluctuations in emission intensity (blinking) typically follows a two-state process, with rather sharp transitions between a distinct *on* and an *off* state.^{15,30,32} By contrast, we always find the presence of a *dim* rather than *off* state in these perovskite crystals, i.e., oscillations in emission intensity occurs on top of some base emission (Figure 6b). Further, more often than not, the emission intensity fluctuates over multiple *bright* states rather than a single *on* state. These observations suggest the presence of multiple emissive sites within each local submicroscopic domain undergoing uncorrelated intensity fluctuations, as would be expected for multiple single nanocrystals within a diffraction limited emissive spot. Alternatively, it is possible that photoexcited carriers undergo migration to specific trap sites (a chemical or a structural defect) where they are quenched nonradiatively,³⁴ and the spatial distribution/density of quenchers in local regions within the crystal can result in a variety of temporal fluctuations over multiple intensity levels.

It is important to note that the PL intermittency (Figure 5) is not exclusively observed for the $\text{MAPbI}_{3-x}(\text{SCN})_x$ micro-crystals, and we also noticed extensive blinking behaviors (of similar characteristics) from localized emission spots within MAPbI_3 microcrystals (see Movies M3 and M4, SI). Therefore, it is reasonable to speculate that such photoinduced optical instability or blinking of emission centers might be a general phenomenon for other perovskite nano/micro-crystals as well. We are currently investigating a wide variety of perovskite materials of different compositions to elucidate the origin of such an intriguing observation.

In conclusion, we demonstrate that incorporation of pseudohalide SCN anions as dopants in MAPbI_3 is a valuable addition to the organic inorganic hybrid perovskite family, with unique optical properties. Quite surprisingly, we find spatially heterogeneous, site specific PL emission from individual $\text{MAPbI}_{3-x}(\text{SCN})_x$ crystals, where the grain boundaries most often exhibit extremely high radiative recombination efficiency as compared to the interior regions. Spatially resolved spectroscopy and lifetime measurements reveal considerable inhomogeneity in the local electronic structures and carrier recombination dynamics among various nanodomains within the interior regions and grain-boundaries. Intriguingly, we have observed unambiguous dynamical fluctuations in emission intensities (blinking) from local nanodomains within micro-crystalline grains for the doped materials as well as the undoped perovskite host. Observation of such PL intermittency is highly unusual for microcrystalline samples and has rarely been observed earlier for perovskite materials. Our results indicate that such a captivating phenomenon may not be compositional or material specific, and can perhaps be generalized for other perovskites as well.

EXPERIMENTAL SECTION

MAPbI_3 precursor solution is prepared by mixing a equimolar ratio of PbI_2 and MAI in DMF, whereas $\text{MAPbI}_{3-x}(\text{SCN})_x$ precursor is prepared dissolving a 1:4 molar ratio of

MAI:Pb(SCN)₂ in DMF. All parent chemicals are purchased off the shelf and used without further purification. Thin films of these samples are prepared by spin-casting these precursors on porous substrates followed by annealing at 363 K for 30 min. These samples are then subjected to XRD measurements directly, whereas for UV-vis and PL measurements, the samples are further encapsulated using spin-casted poly(methyl methacrylate) (PMMA) in chloro-benzene solution to minimize degradation. Photovoltaic device performance (JV characteristics) of $\text{MAPbI}_{3-x}(\text{SCN})_x$ is shown in Figure S9, SI. Further details on the material synthesis, photovoltaic device fabrication, and characterization methodologies are described in the SI.

ASSOCIATED CONTENT

Supporting Information

All experimental details and characterization methodologies are provided along with results from FT-IR, SEM, time-correlated single photon counting (TCSPC), PL microscopy, and spectroscopy. Movies demonstrating blinking are also provided as electronic Supporting Information. The Supporting Information is available free of charge on the ACS Publications website at DOI: 10.1021/acs.jpclett.5b01327.

(PDF)

(MPG)

(MPG)

(MPG)

(MPG)

AUTHOR INFORMATION

Corresponding Authors

*E-mail: shaibal.sarkar@iitb.ac.in.

*E-mail: arindam@chem.iitb.ac.in.

Notes

The authors declare no competing financial interest.

ACKNOWLEDGMENTS

The authors thank the National Center for Photovoltaic Research and Education aided by the Ministry of New and Renewable Energy, Govt. of India, for financial support. We thank Kankan Bhattacharyya for usage of DST (IRPHA), the India funded Centre for Ultrafast Spectroscopy and Microscopy, and Anindya Datta for discussions. A.C. and S.K.S. acknowledge IRCC, IIT Bombay, for initial funding. R.C., S.C., and A.S.S. thank UGC, CSIR, and SERIIUS, respectively, for Ph.D. fellowships.

REFERENCES

- Snaith, H. J. Perovskites: The Emergence of a New Era for Low-Cost, High-Efficiency Solar Cells. *J. Phys. Chem. Lett.* **2013**, *4*, 3623–3630.
- Green, M. A.; Ho-Baillie, A.; Snaith, H. J. The emergence of perovskite solar cells. *Nat. Photonics* **2014**, *8*, 506–514.
- Kamat, P. V. Evolution of Perovskite Photovoltaics and Decrease in Energy Payback Time. *J. Phys. Chem. Lett.* **2013**, *4*, 3733–3734.
- Stranks, S. D.; Eperon, G. E.; Grancini, G.; Menelaou, C.; Alcocer, M. J. P.; Leijtens, T.; Herz, L. M.; Petrozza, A.; Snaith, H. J. Electron-Hole Diffusion Lengths Exceeding 1 Micrometer in an Organometal Trihalide Perovskite Absorber. *Science* **2013**, *342*, 341–344.
- Kim, H.-S.; Mora-Sero, I.; Gonzalez-Pedro, V.; Fabregat-Santiago, F.; Juarez-Perez, E. J.; Park, N.-G.; Bisquert, J. Mechanism of carrier

- accumulation in perovskite thin-absorber solar cells. *Nat. Commun.* **2013**, *4*, 2242.
- (6) Zhao, Y.; Nardes, A. M.; Zhu, K. Solid-State Mesostructured Perovskite $\text{CH}_3\text{NH}_3\text{PbI}_3$ Solar Cells: Charge Transport, Recombination, and Diffusion Length. *J. Phys. Chem. Lett.* **2014**, *5*, 490–494.
 - (7) Lee, M. M.; Teuscher, J.; Miyasaka, T.; Murakami, T. N.; Snaith, H. J. Efficient Hybrid Solar Cells Based on Meso-Superstructured Organometal Halide Perovskites. *Science* **2012**, *338*, 643–647.
 - (8) Kim, H.-S.; Lee, C.-R.; Im, J.-H.; Lee, K.-B.; Moehl, T.; Marchioro, A.; Moon, S.-J.; Humphry-Baker, R.; Yum, J.-H.; Moser, J. E.; Gratzel, M.; Park, N.-G. Lead Iodide Perovskite Sensitized All-Solid-State Submicron Thin Film Mesoscopic Solar Cell with Efficiency Exceeding 9%. *Sci. Rep.* **2012**, *2*, 591.
 - (9) Hodes, G.; Cahen, D. Photovoltaics: Perovskite cells roll forward. *Nat. Photonics* **2014**, *8*, 87–88.
 - (10) Bisquert, J. The Swift Surge of Perovskite Photovoltaics. *J. Phys. Chem. Lett.* **2013**, *4*, 2597–2598.
 - (11) Eperon, G. E.; Stranks, S. D.; Menelaou, C.; Johnston, M. B.; Herz, L. M.; Snaith, H. J. Formamidinium lead trihalide: a broadly tunable perovskite for efficient planar heterojunction solar cells. *Energy Environ. Sci.* **2014**, *7*, 982.
 - (12) Jiang, Q.; Rebollar, D.; Gong, J.; Piacentino, E. L.; Zheng, C.; Xu, T. Pseudohalide-Induced Moisture Tolerance in Perovskite $\text{CH}_3\text{NH}_3\text{Pb}(\text{SCN})_2\text{I}$ Thin Films. *Angew. Chem., Int. Ed.* **2015**, *54*, 7617–7620.
 - (13) Iwade, Y.; Kawamura, K.; Igarashi, K.; Mochinaga, J. Effective ionic radii of nitrite and thiocyanate estimated in terms of the Boettcher equation and the Lorentz-Lorenz equation. *J. Phys. Chem.* **1982**, *86*, 5205–5208.
 - (14) deQuilettes, D. W.; Vorpahl, S. M.; Stranks, S. D.; Nagaoka, H.; Eperon, G. E.; Ziffer, M. E.; Snaith, H. J.; Ginger, D. S. Impact of microstructure on local carrier lifetime in perovskite solar cells. *Science* **2015**, *348*, 683–686.
 - (15) Stefani, F. D.; Hoogenboom, J. P.; Barkai, E. Beyond quantum jumps: Blinking nanoscale light emitters. *Phys. Today* **2009**, *62*, 34–39.
 - (16) Qiu, J.; Qiu, Y.; Yan, K.; Zhong, M.; Mu, C.; Yan, H.; Yang, S. All-solid-state hybrid solar cells based on a new organometal halide perovskite sensitizer and one-dimensional TiO_2 nanowire arrays. *Nanoscale* **2013**, *5*, 3245–8.
 - (17) Chen, Q.; Zhou, H.; Fang, Y.; Stieg, A. Z.; Song, T.-B.; Wang, H.-H.; Xu, X.; Liu, Y.; Lu, S.; You, J.; Sun, P.; McKay, J.; Goorsky, M. S.; Yang, Y. The optoelectronic role of chlorine in $\text{CH}_3\text{NH}_3\text{PbI}_3(\text{Cl})$ -based perovskite solar cells. *Nat. Commun.* **2015**, *6*, 7269.
 - (18) Lee, K.-K.; Park, K.-H.; Kwon, D.; Choi, J.-H.; Son, H.; Park, S.; Cho, M. Ion-pairing dynamics of Li^+ and SCN^- in dimethylformamide solution: Chemical exchange two-dimensional infrared spectroscopy. *J. Chem. Phys.* **2011**, *134*, 064506.
 - (19) Jeon, N. J.; Noh, J. H.; Kim, Y. C.; Yang, W. S.; Ryu, S.; Seok, S. I. Solvent engineering for high-performance inorganic–organic hybrid perovskite solar cells. *Nat. Mater.* **2014**, *13*, 897–903.
 - (20) Colella, S.; Mosconi, E.; Fedeli, P.; Listorti, A.; Gazza, F.; Orlandi, F.; Ferro, P.; Besagni, T.; Rizzo, A.; Calestani, G.; Gigli, G.; De Angelis, F.; Mosca, R. $\text{MAPbI}_{3-x}\text{Cl}_x$ Mixed Halide Perovskite for Hybrid Solar Cells: The Role of Chloride as Dopant on the Transport and Structural Properties. *Chem. Mater.* **2013**, *25*, 4613–4618.
 - (21) Butler, K. T.; Frost, J. M.; Walsh, A. Band alignment of the hybrid halide perovskites $\text{CH}_3\text{NH}_3\text{PbCl}_3$, $\text{CH}_3\text{NH}_3\text{PbBr}_3$ and $\text{CH}_3\text{NH}_3\text{PbI}_3$. *Mater. Horiz.* **2015**, *2*, 228–231.
 - (22) Wehrenfennig, C.; Liu, M.; Snaith, H. J.; Johnston, M. B.; Herz, L. M. Homogeneous Emission Line Broadening in the Organo Lead Halide Perovskite $\text{CH}_3\text{NH}_3\text{PbI}_{3-x}\text{Cl}_x$. *J. Phys. Chem. Lett.* **2014**, *5*, 1300–1306.
 - (23) Wehrenfennig, C.; Liu, M.; Snaith, H. J.; Johnston, M. B.; Herz, L. M. Charge carrier recombination channels in the low-temperature phase of organic-inorganic lead halide perovskite thin films. *APL Mater.* **2014**, *2*, 081513.
 - (24) Wu, K.; Bera, A.; Ma, C.; Du, Y.; Yang, Y.; Li, L.; Wu, T. Temperature-dependent excitonic photoluminescence of hybrid organometal halide perovskite films. *Phys. Chem. Chem. Phys.* **2014**, *16*, 22476–81.
 - (25) Deschler, F.; Price, M.; Pathak, S.; Klintberg, L. E.; Jarausch, D.-D.; Higler, R.; Hüttner, S.; Leijtens, T.; Stranks, S. D.; Snaith, H. J.; Ataüre, M.; Phillips, R. T.; Friend, R. H. High Photoluminescence Efficiency and Optically Pumped Lasing in Solution-Processed Mixed Halide Perovskite Semiconductors. *J. Phys. Chem. Lett.* **2014**, *5*, 1421–1426.
 - (26) De, S.; Layek, A.; Raja, A.; Kadir, A.; Gokhale, M. R.; Bhattacharya, A.; Dhar, S.; Chowdhury, A. Two Distinct Origins of Highly Localized Luminescent Centers within InGaN/GaN Quantum-Well Light-Emitting Diodes. *Adv. Funct. Mater.* **2011**, *21*, 3828–3835.
 - (27) Layek, A.; De, S.; Thorat, R.; Chowdhury, A. Spectrally Resolved Photoluminescence Imaging of ZnO Nanocrystals at Single-Particle Levels. *J. Phys. Chem. Lett.* **2011**, *2*, 1241–1247.
 - (28) Stranks, S. D.; Burlakov, V. M.; Leijtens, T.; Ball, J. M.; Goriely, A.; Snaith, H. J. Recombination Kinetics in Organic-Inorganic Perovskites: Excitons, Free Charge, and Subgap States. *Phys. Rev. Appl.* **2014**, *2*, 034007.
 - (29) Christians, J. A.; Manser, J. S.; Kamat, P. V. Multifaceted Excited State of $\text{CH}_3\text{NH}_3\text{PbI}_3$. Charge Separation, Recombination, and Trapping. *J. Phys. Chem. Lett.* **2015**, *6*, 2086–2095.
 - (30) Nirmal, M.; Dabbousi, B. O.; Bawendi, M. G.; Macklin, J. J.; Trautman, J. K.; Harris, T. D.; Brus, L. E. Fluorescence intermittency in single cadmium selenide nanocrystals. *Nature* **1996**, *383*, 802–804.
 - (31) Dickson, R. M.; Cubitt, A. B.; Tsien, R. Y.; Moerner, W. E. On/off blinking and switching behaviour of single molecules of green fluorescent protein. *Nature* **1997**, *388*, 355–358.
 - (32) Aoki, T.; Nishikawa, Y.; Kuwata-Gonokami, M. Room-temperature random telegraph noise in luminescence from macroscopic InGaN clusters. *Appl. Phys. Lett.* **2001**, *78*, 1065–1067.
 - (33) Micheletto, R.; Abiko, M.; Kaneta, A.; Kawakami, Y.; Narukawa, Y.; Mukai, T. Observation of optical instabilities in the photoluminescence of InGaN single quantum well. *Appl. Phys. Lett.* **2006**, *88*, 061118.
 - (34) Tian, Y.; Merdasa, A.; Peter, M.; Abdellah, M.; Zheng, K.; Ponseca, C. S.; Pullerits, T.; Yartsev, A.; Sundström, V.; Scheblykin, I. G. Giant Photoluminescence Blinking of Perovskite Nanocrystals Reveals Single-Trap Control of Luminescence. *Nano Lett.* **2015**, *15*, 1603–1608.